Chemical Transformations in Individual Ultrasmall Biomimetic Containers

Daniel T. Chiu,[1] Clyde F. Wilson,[1] Frida Ryttsén,[2] Anette Strömberg,[2] Cecilia Farre,[2] Anders Karlsson,[2] Sture Nordholm,[2] Anuj Gaggar,[1] Biren P. Modi,[1] Alexander Moscho,[1] Roberto A. Garza-López,[3] Owe Orwar,[2] Richard N. Zare[1]*

Individual phospholipid vesicles, 1 to 5 micrometers in diameter, containing a single reagent or a complete reaction system, were immobilized with an infrared laser optical trap or by adhesion to modified borosilicate glass surfaces. Chemical transformations were initiated either by electroporation or by electrofusion, in each case through application of a short (10-microsecond), intense (20 to 50 kilovolts per centimeter) electric pulse delivered across ultramicroelectrodes. Product formation was monitored by far-field laser fluorescence microscopy. The ultrasmall characteristic of this reaction volume led to rapid diffusional mixing that permits the study of fast chemical kinetics. This technique is also well suited for the study of reaction dynamics of biological molecules within lipid-enclosed nanoenvironments that mimic cell membranes.

Living systems usually carry out biochemical transformations within cellular compartments defined by a phospholipid bilayer boundary. At such small dimensions [zeptoliters (10^{-21} liters) to femtoliters (10^{-15} liters)], the surface-to-volume ratio is very high and the contained molecules experience collisions with the phospholipid surface at high frequencies. A hard-sphere approximation and a simulation of Brownian motion indicate that, in a 170-nm-diameter vesicle, a single enzyme and a single substrate collide at a frequency of 300 kHz, which might be compared with the substrate-wall collisional frequency of 200 MHz (*1*). Thus, the biochemical reactivity of the contained molecules can be dominated by surface interactions, and such interactions can profoundly influence enzyme kinetics (*2*). A tool to study confined chemical reactions under biologically relevant conditions would offer valuable insights into in vivo reaction conditions.

Various approaches exist for carrying out chemical reactions in aqueous solutions at small dimensions (*3*–*7*). Most open volume methods involve micromachining techniques (*4*) by which nanoliter to femtoliter wells can be created in silicon-based substrates (*5*). For self-enclosed volume elements, microdroplets in an immiscible solvent have been used (*6*). However, these techniques do not create the biologically relevant nanoenvironment that can be achieved in lipid vesicles.

From the perspective of chemical kinetics (*7, 8*), this method also offers the ability to achieve rapid diffusional mixing (microsecond to millisecond time range), and it opens the opportunity to study fast chemical reaction kinetics that are inaccessible to traditional bulk turbulence mixing techniques. The diffusive mixing time of dye molecules is about 8 ms for a 2-μm vesicle and 20 μs for a 0.1-μm vesicle. The small volume element contained within individual vesicles also matches the probe volume dimension of many optical single-molecule detection and manipulation schemes (*9*).

Using a recently developed rotaevaporative technique, we prepared unilamellar vesicles between 50 nm and 50 μm in diameter from a wide range of different phospholipids (*10*). The vesicles can encapsulate one or more reagent molecules of choice. Purified vesicle preparations are transferred to a bare or poly-L-lysine–coated borosilicate cover slip mounted on the stage of an inverted fluorescence microscope. Attoliter to zeptoliter vesicles can be precisely positioned and manipulated in solution by optical trapping (*11*). We used micromanipulator-controlled ultramicroelectrodes for electroporation and electrofusion, an infrared laser for optical trapping, two lasers (Ar^+ and HeNe) for excitation, and two independent detection channels (Fig. 1). Optical damage to the vesicles has been observed at high laser powers and short wavelengths (ultraviolet). The power used for laser-induced fluorescence, however, is not sufficient to induce membrane damage, especially in the visible region where the lipid bilayer lacks absorption features. The membrane integrity of vesicles is also very sensitive to buffer conditions, such as ionic strength, pH, and type of buffer used.

Figure 2 illustrates the hydrolysis of fluorescein diphosphate catalyzed by alkaline phosphatase. Fluorescein dianion product inside an optically trapped 3-μm vesicle was

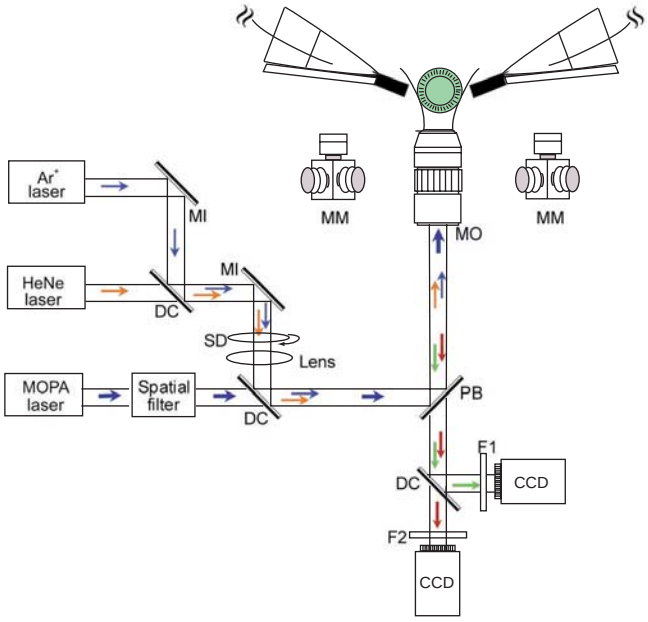

Fig. 1. Schematic of the experimental setup. Two carbon-fiber electrodes (5 μm in diameter) controlled by micromanipulators (MM) were used for electroporation and electrofusion. Three colinear laser beams were sent into a ×100, 1.3 numerical aperture microscope objective (MO). The 488-nm output of an argon ion laser (blue arrows) causes excitation of carboxyrhodamine-6G, Ca^{2+}-chelated fluo-3, and fluorescein. The 633-nm output of a HeNe laser (orange arrows) causes excitation of TOTO-3–intercalated DNA. The 992-nm output of a MOPA diode laser (black arrows) is used for optical trapping of vesicles. The resulting dye fluorescence (green and red arrows) is collected, separated by a dichroic beamsplitter (DC) into two different color channels, passed through a bandpass filter (F1 or F2), and then detected by one of two CCD cameras. This setup is also modified to operate in a confocal mode with a single-photon counting silicon avalanche diode detector. MI, mirror; PB, polychroic beamsplitter; SD, spinning disk.

[1]Department of Chemistry, Stanford University, Stanford, CA 94305, USA. [2]Department of Chemistry, Göteborg University, Göteborg, SE-41296, Sweden. [3]Department of Chemistry, Pomona College, Claremont, CA 91711, USA.

*To whom correspondence should be addressed.

monitored by confocal fluorescence microscopy (*9*) at 60-s intervals. The time zero of the reaction for each interval is set by bleaching any products present. A nondestructive alternative to photobleaching is to monitor the product buildup over time. The small dynamic range of our detection scheme, however, prevented the use of this approach. Fewer than 100 product chromophores were produced between the time of bleaching and detection. With further optimization, formation of single product chromophores could be followed in real time—for example, by using fluorescence detection.

Because of the small volume element in a vesicle, the initial number of substrate molecules is limited and typically becomes largely depleted during the time required to prepare the vesicle. One way to overcome this drawback is to use the lipid bilayer as a partition between the reactants. The reaction can then be initiated by breaking down the bilayer through electric field–mediated membrane pore formation or membrane fusion.

Pore formation in lipid bilayers typically occurs within 50 μs (*12, 13*) and is controlled by the applied electric field strength and pulse duration; resealing of the membrane occurs in microseconds and sometimes longer (*12, 14*). To electroporate reagents into individual reagent-encapsulated vesicles and to perform electrofusion on single vesicle partners, we developed a miniaturized version of electroporation and electrofusion for individual vesicles. From whole-vesicle patch clamp measurements, we found that pore formation after electroporation was rapid. The inward current was observed to reach its half-maximal value after 276 ± 31 μs. The shape of the curve (Fig. 3) shows striking similarities to studies on irreversible electrical breakdown of unilamellar planar lipid films (*15*). In addition, when phosphatidylcholine (PC) vesicles containing 50 μM fluorescein and 150 mM NaCl (pH 7.2) surrounded by a citrate buffer (pH 4.3) were electroporated, we found a similar temporal dependence for quenching of fluorescence from intravesicular fluorescein (Fig. 3). During the pore-opening time, H^+ ions diffuse into the liposome and protonate the fluorescein dianions, causing fluorescence quenching. Control experiments, in which the pH was adjusted to 8 both inside and outside the vesicle, did not result in any decreased fluorescence during electroporation (Fig. 3, insets). To drive the selective influx of molecules into the vesicles, we can exploit both concentration gradients and size differences between the molecules inside and outside the vesicle. Much faster pore-opening kinetics has been achieved in some lipid systems, which could enable reactions to be studied on low-microsecond time scales (*12–14*). In addition, vesicles with dimensions of tens of nanometers can be prepared, which also opens the possibility of low-microsecond diffusive mixing times.

Electroporation is useful in initiating reactions with sharp time distributions, but it lacks the capability to control precisely the amount of reagents delivered. In contrast, electrofusion between two select vesicles can be used to mix precise amounts of reagents. Optical traps (*11*) were used to align two selected vesicles for fusion. Fusion, induced by the reversible dielectric breakdown of the bilayer membrane (*15–18*), is achieved by application of a short, intense, and highly directed electric field generated across a pair of carbon-fiber ultramicroelectrodes (1- to 5-μm tip diameter). Pulses with a duration of 10 to 30 μs and an electric field strength of 20 to 50 kV/cm provided a near unity fusion yield. Figure 4A is a frequency histogram showing the number of pulses required to achieve fusion in 28 separate trials. About 14% of the fusions occurred after only one pulse and >70% of fusions occurred within five pulses (*19*).

The initial stages of electrofusion are similar to electroporation. Fusion pores are being generated in the process. To determine whether leakage limits the utility of this

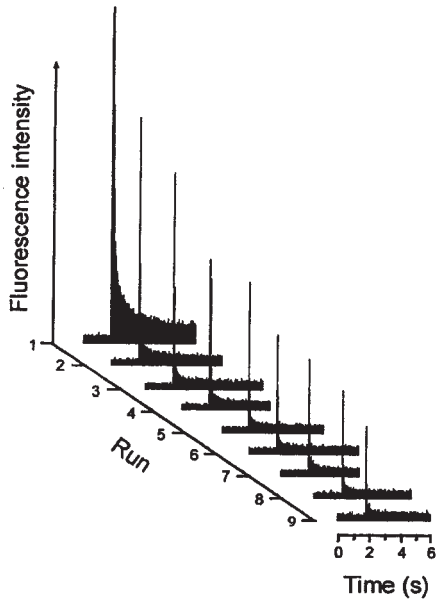

Fig. 2. Fluorescence intensity versus time as a measure of alkaline phosphatase (AP) catalytic activity inside an optically trapped 3-μm vesicle containing AP and fluorescein diphosphate (0.75 mM). At 60-s intervals, the amount of fluorescent product accumulated after bleaching at the same wavelength is probed at 488 nm. The bleaching resets the reaction clock for each run. The peak values for each run were fitted to an exponential function, $y = A \exp(-kx)$, with $A = 1118.6$, $k = 0.198$, and a correlation coefficient of 0.98.

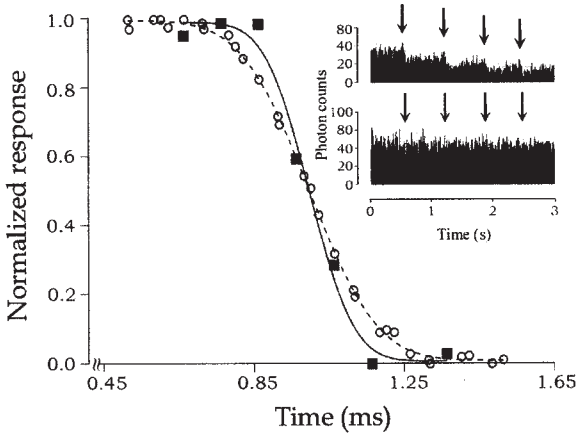

Fig. 3. Electroporation of single vesicles. Electric field–induced (20 V, 10 μs) membrane breakdown is measured by using patch clamp recordings (open circles), which are fit to a function describing a statistical sigmoid. The time needed for the current to reach its half-maximum value is 276 ± 31 μs ($N = 6$). Vesicles (10 μm in diameter) made from 74% PC, 19% phosphatidic acid, 7% cholesterol are patched in the whole-vesicle configuration and clamped to a holding potential of −10 to −30 mV. Ultramicroelectrodes are placed on opposite sides of the vesicle at an interelectrode distance of about 35 μm. Bath and pipette solutions are 140 mM NaCl and 10 mM Hepes (pH 7.4). Patch clamp data are sampled and stored on videotape (digitized at 20 kHz, filter frequency 10 kHz) and analyzed without additional filtering of the signal. In the fluorescence measurements (solid squares), 1- to 10-μm-diameter PC vesicles containing 50 μM fluorescein (pK_a 6.5, where K_a is the acid constant) in 150 mM NaCl (pH 7.2) are electroporated (25 V, 10 μs duration) in a citrate buffer (pH 4.3). The start pulse from the multichannel scalar electronically triggers and initiates electroporation, which helps us define time zero of the experiment. The signal was detected with a single photon-counting module (50-μs dwell time per channel), filtered by using a five-point Savitsky–Golay smoothing algorithm, and normalized. The time needed for the fluorescence to reach its half-maximum value was determined to be about 184 μs. The figure shows a sigmoidal fit of the decrease in fluorescence intensity from the electroporated vesicles (average of four experiments). The fluorescence and patch clamp curves were centered at $t = 1.0$ ms where the sigmoidal curves reached 50% of their maximal values. (**Inset**) Full-trace scans from electroporation (25 V, 10-μs duration) of a fluorescein-containing vesicle (pH 8 inside) in an acidic solution (upper) (600-μs dwell time per channel) and in a solution buffered at the same pH (lower) (800-ms dwell time per channel). In the upper trace the fluorescence decreases because of the inflow of protons from the surrounding solution after electroporation, as indicated by arrows. No such events can be detected in the lower trace after electroporation (arrows).

technique, we encapsulated fluorescent molecules into the vesicles and monitored the fluorescence of these molecules before and after fusion under low-intensity excitation to minimize photoinduced bleaching of the chromophores. The fluorescence recovery as a function of the number of pulses is plotted (Fig. 4B), and the fluorescence images of two vesicles before and after fusion are shown (Fig. 4B, insets). On average, more than 94% of the fluorescence remained for one-pulse fusions (see also Fig. 4B, insets). Even for fusions that required more than 10 pulses, the vesicle still retained 60% or more of its fluorescence. We conclude that pores are formed when the two vesicles are fused, but the pores open and close too rapidly for any substantial amount of dye molecules to escape.

To demonstrate mixing after fusion, we fused two vesicles, each containing a different fluorescent dye (Fig. 5, A to D). To perform two-color mixing in fluorescence, we simultaneously excited the contents of the fused vesicle with two different wavelengths. The emitted photons were collected and separated into their respective color channels and then detected by two charge-coupled device (CCD) cameras (see Fig 1). Figure 5 shows the fusion between a vesicle containing carboxyrhodamine-6G (green fluorescence) and one containing TOTO-3-intercalated 15-mer DNA (red fluorescence) to yield a fused vesicle that appears orange.

Figure 5, E to H, shows a chemical reaction carried out inside these ultrasmall containers, one of which holds fluo-3 (10 μM) and the other Ca^{2+} (10 μM). Before fusion (Fig. 5G), no fluorescence was detected from the Ca^{2+}-containing vesicle, but a small background fluorescence was observed in the vesicle with fluo-3. Binding of Ca^{2+} by fluo-3 increases the fluorescence quantum yield of this chelator by about 40-fold (*20*). This fluorescence enhancement was indeed observed, as demonstrated in Fig. 5H, which represents the image taken after the contents of the two vesicles were mixed and the chelating reaction was initiated. Although we focused on fluorogenic reactions and fluorescence quenching in our experiments, other optical techniques might also be used, including measurement of polarization, lifetime, and fluorescence energy transfer.

The technique we have described offers the special opportunity to probe the dynamics of chemical reactions in spatially confined biomimetic nanoenvironments. By systematically varying the membrane lipid, protein, and glycoprotein composition of a vesicle, the in vivo activity of multiple or single biological molecules might be inferred. In combination with single-molecule detection (*9*) and manipulation methodologies (*11*), single-molecule reactions can be studied within the lipid bilayer boundary of a vesicle. Because only one reaction is studied at a time, synchronization of the reactions is not necessary. Therefore, the observable chemical kinetics is limited only by the excited-state lifetime of the chromophore. The small volume characteristics of this technique should also find use as a general chemical or biochemical delivery system whose spatial and temporal locations can be precisely controlled.

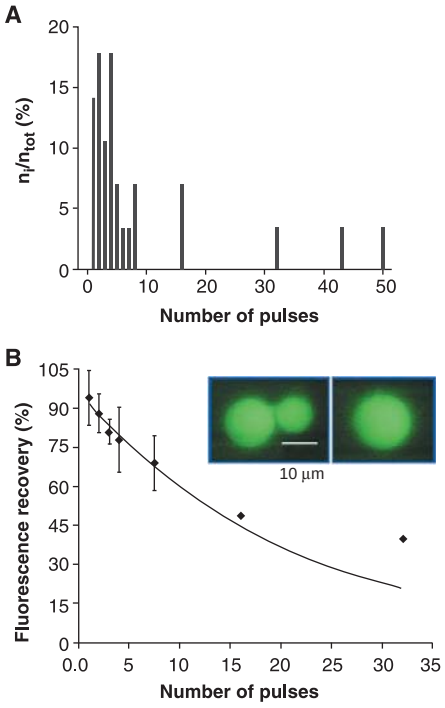

Fig. 4. (**A**) Histogram of the number of pulses required to achieve fusion (28 trials). The electric-field pulse is rectangular with a field strength of 40 kV/cm and a duration of 30 μs. Pulses were applied to PC vesicles containing fluorescein (0.1 mM) in a 10 mM Hepes buffer with 140 mM NaCl (pH 8). (**B**) Fluorescence recovery versus number of pulses applied. Data with error bars are mean values ± standard deviations (n = 3 to 5) and were fitted to a single exponential decay plotted for the entire data set. Data without error bars are single measurements. The fluorescence recovery is calculated as fluorescence intensity ratio of the product liposome to the arithmetic sum of the vesicles before fusion. (**Insets**) Images before and after fusion taken in fluorescence (488-nm excitation).

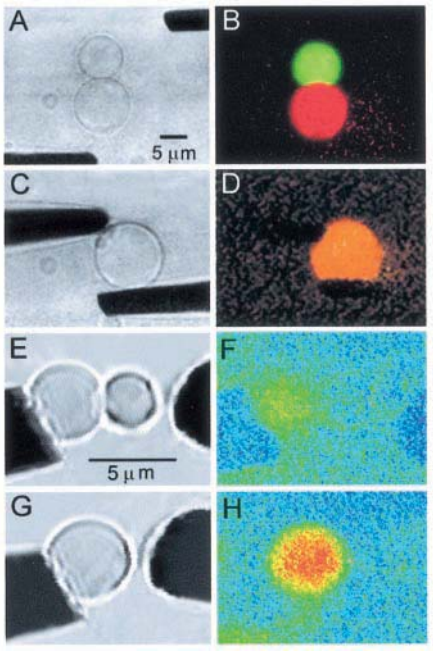

Fig. 5. (**A** to **D**) Fluorescence color mixing. Fusion of two vesicles, each containing a dye whose fluorescence is at a different color: 20 μM carboxyrhodamine-6G (top vesicle) and 20 μM TOTO-3–intercalated 15-mer DNA (bottom vesicle). (A) and (C) are bright-field images taken before and after fusion; (B) and (D) are the corresponding fluorescence images, obtained as described in Fig. 1. The buffer and pulse conditions were similar to those in Fig. 4. Images before (**E**) and after (**G**) electrofusion (about 75 kV/cm; 10 μs) of a 10 μM fluo-3–containing vesicle (left) and a 10 μM Ca^{2+}-containing vesicle (right) are shown under bright-field illumination in a buffer solution containing 10 mM Hepes and 140 mM NaCl (pH 7.4). Corresponding fluorescence images are shown in (**F**) and (**H**). The fluo-3 solution encapsulated in the liposomes and the extraliposomal solution were titrated with EGTA to reduce background fluorescence. The vesicles were initially immobilized on poly-L-lysine–coated borosilicate cover slips, followed by rinsing with Ca^{2+}-free buffer solution.

References and Notes

1. We used a Brownian dynamics simulation program, in which we treated a single enzyme and a single substrate as hard spheres. The radius of each molecule was estimated from the Stokes–Einstein law as described [D. L. Ermak, *J. Chem. Phys.* **62**, 4189 (1975)]. The diffusion constants for the molecules were modeled by changing the time steps taken by the molecules and the constant velocities given to them. The trajectories were followed and the diffusion constants were calculated as described [P. Turq, F. Lantalme, H. L. Friedman, *J. Chem. Phys.* **66**, 3039 (1977)]. We used D(enzyme) = 7×10^{-11} m^2 s^{-1} and D(substrate) = 4.4×10^{-10} m^2 s^{-1}. This model was later used to obtain an estimate of the number of collisions between enzyme and substrate and also between the different molecules and the phospholipid wall, which was treated as a hard wall. Substrate-wall collisions scale as $1/r$ and substrate-enzyme collisions scale as $1/r^3$, where r is the vesicle radius.
2. J. Drott, L. Rosengren, K. Lindström, T. Laurell, *Thin Solid Films* **330**, 161 (1998).
3. C.-Y. Kung, M. D. Barnes, N. Lermer, W. B. Whitten, J. M. Ramsey, *Anal. Chem.* **70**, 658 (1998).
4. G. T. A. Kovacs, K. Petersen, M. Albin, *ibid.* **68**, 407A (1996).
5. A. J. You, R. J. Jackman, G. M. Whitesides, S. L. Schreiber, *Chem. Biol.* **4**, 969 (1997); R. A. Clark, R. B. Hietpas, A. G. Ewing, *Anal. Chem.* **69**, 259 (1997); W. Tan and E. S. Yeung, *ibid.*, p. 4242.
6. H. Masuhara, Ed., *Microchemistry: Spectroscopy and Chemistry in Small Domains, Proceedings of the JRDC-KUL Joint International Symposium on Spectroscopy and Chemistry* (North-Holland, Amsterdam, 1994); S. Funakura, K. Nakatani, H. Misawa, W. Kitamura, H. Masuhara, *J. Phys. Chem.* **98**, 3073 (1994); B. Rotman, *Proc. Natl. Acad. Sci. U.S.A.* **47**, 1981 (1961).
7. K. Jensen, *Nature* **393**, 735 (1998).
8. J. B. Knight, A. Vishwanath, J. P. Brody, R. H. Austin, *Phys. Rev. Lett.* **80**, 3863 (1998).
9. S. Nie and R. N. Zare, *Annu. Rev. Biophys. Biomol.*

Struct. **26**, 567 (1997); D. T. Chiu and R. N. Zare, *Chem. Eur. J.* **3**, 335 (1997).
10. A. Moscho, O. Orwar, D. T. Chiu, B. P. Modi, R. N. Zare, *Proc. Natl. Acad. Sci. U.S.A.* **93**, 11443 (1996). The reagent molecules of interest are introduced into the vesicles during the formation process. A main advantage of this preparative technique is speed; unilamellar vesicles can be prepared within 2 min. This advantage is particularly important for encapsulating and reacting labile molecules for which long preparation times might lead to degradation. Another important advantage is the flexibility of the technique: the internal and external buffer solution, reaction chamber size, and reaction chamber surface properties can be easily varied to mimic the particular cell types or organelles of interest.
11. D. T. Chiu *et al.*, *Anal. Chem.* **69**, 1801 (1997).
12. Chernomordik *et al.*, *Biochim. Biophys. Acta* **902**, 360 (1987).
13. C. Wilhelm, M. Winterhalter, U. Zimmermann, R. Benz, *Biophys. J.* **64**, 121 (1993).
14. D. C. Chang and T. S. Reese, *ibid.* **58**, 1 (1990).
15. U. Zimmermann, *Biochim. Biophys. Acta* **694**, 227 (1982); N. G. Stoicheva and S. W. Hui, *ibid.* **1195**, 31 (1994); S. W. Hui and D. A Stenger, *Methods Enzymol.* **220**, 212 (1993).
16. N. Düzgünes and J. Wilschut, *Methods Enzymol.* **220**, 3 (1993).
17. The electrically induced poration or fusion of cells is used extensively in biological research for introduction of molecules or genes into cells or for creation of new cell lines (*15*). These experiments typically are performed in a chamber, in a random manner, where several million cells are electroporated or fused simultaneously, with a relatively low yield. In our experiments, we extend the use of this physical principle to the level of single vesicles with subcellular dimensions. This extension is made possible by the use of a highly localized electric field from a pair of ultramicroelectrodes, precise manipulation techniques, and sensitive laser-induced fluorescence detection.
18. D. A. Stenger and S. W. Hui, *Biophys. J.* **53**, 833 (1988); D. Needham, *Methods Enzymol.* **220**, 111 (1993).
19. Electroporation and electrofusion of vesicles are relatively straightforward to perform. The procedure of selecting, isolating, and aligning two vesicles of different contents before fusion, however, requires some skill and experience. This procedure might be simplified by using micromachined channels and wells as conduits for selection and isolation of vesicles.
20. R. Y. Tsien, *Annu. Rev. Neurosci.* **12**, 227 (1989).
21. Supported by New Energy and Industrial Technology Development Organization of Japan under the International Joint Research Program, the U.S. National Institute on Drug Abuse (DA09873), the Swedish Foundation for Strategic Research (5SF), and the Swedish Natural Science Research Council (NFR) (10481-305-308 and -309). We thank S. Orwar for technical assistance with image processing. C.F.W. acknowledges support from the Stanford Graduate Fellowship. A.G. and B.P.M. are Stanford University Bing Chemistry Summer Undergraduate Research Fellows. B.P.M. acknowledges funding by a Howard Hughes Summer Fellowship from the Stanford University Department of Biological Sciences.

13 April 1998; accepted 16 February 1999

Nonequilibrium Self-Assembly of Long Chains of Polar Molecules in Superfluid Helium

K. Nauta and R. E. Miller*

It is shown that in the low-temperature (0.37 kelvin) environment of superfluid helium droplets, long-range dipole-dipole forces acting between two polar molecules can result in the self-assembly of noncovalently bonded linear chains. At this temperature the effective range of these forces is on the nanometer scale, making them important in the growth of nanoscale structures. In particular, the self-assembly of exclusively linear hydrogen cyanide chains is observed, even when the folded structures are energetically favored. This suggests a design strategy for the growth of new nanoscale oligomers composed of monomers with defined dipole (or higher order) moment directions.

It is well known that as two point dipoles approach from long range they prefer to orient in a head-to-tail configuration (*1*). An analogous and perhaps more familiar case is that of two approaching magnets that orient such that their north poles point in the same direction. These simple ideas would lead one to predict that highly polar monomer units might assemble head-to-tail to form linear polymer chains. However, at room temperature the average rotational energy is large relative to the dipole-dipole interactions, such that the $1/R^3$ interaction (R being the distance between the dipoles) motionally averages (integrated over all angles) to $1/R^6$ (*2*), greatly reducing its range. As a result, dipole-dipole forces generally play only a minor role in determining the local "structure" of simple liquids (*2*). Chainlike structures are seen in some polar solids, such as crystalline HCN (*3*). However, the lateral dispersion interactions between chains (the crystal force field) are important in stabilizing such structures, and it is not obvious that they will be stable in the gas phase, where more compact structures better optimize the weak interactions between the molecules. We might therefore expect that the strong dipole-dipole interactions will dominate only for short chains and that the energy penalty for keeping the system linear will increase with chain length to the point where the system eventually folds. Ab initio calculations have been performed for isolated HCN complexes that confirm this general trend (*4–6*).

In this study we show that polar monomers can self-assemble exclusively into extended linear chains in superfluid liquid helium droplets. These droplets represent a spectroscopic matrix (*7*) with many interesting properties, including a low-temperature (0.37 K) (*8*) and a weakly interacting and homogeneous environment that results in small vibrational frequency shifts and high spectral resolution (sufficient to show rotational structure) for solvated molecules (*8–11*). Hydrogen cyanide was chosen for this study because of its large dipole moment (3 D) and the existence of previous gas-phase studies of its complexes (*12–15*).

In our experimental apparatus (Fig. 1), the helium droplet source consists of a 5-μm-diameter nozzle operated at about 20 K, through which ultrapure helium is expanded from a pressure of 50 bar. Under these conditions helium droplets with a mean diameter of about 7 nm (4000 atoms) are formed. These droplets then pass through a pick-up cell maintained at an HCN pressure between 10^{-6} and 10^{-5} mbar. In this region, HCN molecules are captured individually by the helium droplets and cooled to 0.37 K (*8*, *10*). The seeded droplets then pass through the laser excitation region and are detected by either the bolometer (*16*) or mass spectrometer. Vibrational excitation and relaxation of the molecules in the helium droplet result in the evaporation of several hundred helium atoms, reducing the total flux to the detectors. The electrodes shown in Fig. 1 were used to apply a large electric field to the laser excitation region. The resulting pendular-state spectroscopy (*17*) was an essential part of assigning the spectra of the polar chains.

In a gas-phase free jet expansion the most stable isomer of a complex tends to form, and therefore the experimentally determined geometry is often the same as the ab initio global minimum structure. Only when there are a number of isomers with similar energies does one expect to observe the formation of more than one of them (*18*, *19*). This can be explained by noting that the clusters are formed in the high-density, relatively hot region of the expansion where there is still sufficient energy to surmount any barriers on the potential energy surface to reach the global minimum. Subsequent two-body collisions with the carrier gas then cool the complex to the very low temperatures typical of free jet expansions (~1 K), thereby trapping the system in the global minimum. The HCN trimer

Department of Chemistry, University of North Carolina, Chapel Hill, NC 27599, USA.

*To whom correspondence should be addressed. E-mail: remiller@unc.edu